Journal of Materials Chemistry A

Accepted Manuscript

ROYAL SOCIETY OF CHEMISTRY

www.rsc.org/materialsA

HIGH-TEMPERATURE CHARACTERIZATION OF OXYGEN-DEFICIENT K_2NiF_4-TYPE $Nd_{2-x}Sr_xNiO_{4-\delta}$ (x = 1.0-1.6) FOR POTENTIAL SOFC/SOEC APPLICATIONS

Ekaterina Kravchenko [a,b], Dmitry Khalyavin [c], Kiryl Zakharchuk [a], Jekabs Grins [d], Gunnar Svensson [d], Vladimir Pankov [b], Aleksey Yaremchenko [a] *

[a] CICECO, Department of Materials and Ceramic Engineering, University of Aveiro, 3810-193 Aveiro, Portugal

[b] Department of Chemistry, Belarusian State University, Leningradskaya 14, 220030 Minsk, Belarus

[c] ISIS Facility, Rutherford Appleton Laboratory, Harwell Oxford, Didcot, OX11 0QX, United Kingdom

[d] Department of Materials and Environmental Chemistry, Stockholm University, SE-106 91Stockholm, Sweden

* Corresponding author. Fax: +351-234-370204; Tel: +351-234-370235;
E-mail: ayaremchenko@ua.pt

† Electronic supplementary information (ESI) available.

Table of Contents Entry

Substitution by strontium induces significant oxygen deficiency in crystal lattice of K_2NiF_4-type $Nd_{2-x}Sr_xNiO_{4-\delta}$ at elevated temperatures which, in combination with significant electronic conductivity, implies enhanced mixed ionic-electronic transport favorable for electrode applications

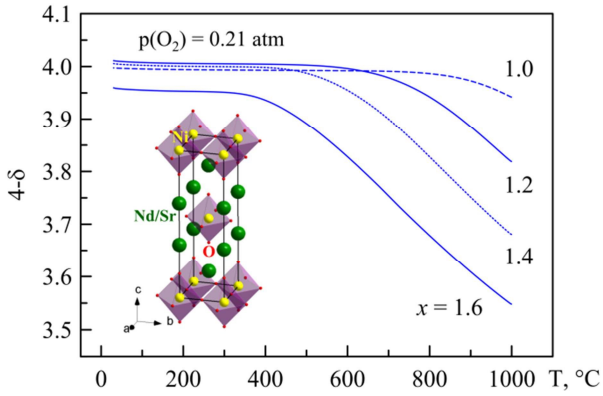

Abstract

Previously unexplored oxygen-deficient Ruddlesden-Popper $Nd_{2-x}Sr_xNiO_{4-\delta}$ (x = 1.0-1.6) nickelates were evaluated for potential use as oxygen electrode materials for solid oxide fuel and electrolysis cells, with emphasis on structural stability, oxygen nonstoichiometry, dimensional changes, and electrical properties. $Nd_{2-x}Sr_xNiO_{4-\delta}$ ceramics possess K_2NiF_4-type tetragonal structure under oxidizing conditions at 25-1000°C. Acceptor-type substitution by strontium is compensated by the generation of electron-holes and oxygen vacancies. Oxygen deficiency increases with temperature and strontium doping reaching ~1/8 of oxygen sites for x = 1.6 at 1000°C in air. Strongly anisotropic expansion of tetragonal lattice on heating correlated with oxygen nonstoichiometry changes results in an anomalous dilatometric behavior of $Nd_{2-x}Sr_xNiO_{4-\delta}$ ceramics under oxidizing conditions. Moderate thermal expansion coefficients, $(11\text{-}14)\times10^{-6}$ K^{-1}, ensure however thermomechanical compatibility with common solid electrolytes. Reduction in inert atmosphere induces oxygen vacancy ordering accompanied with a contraction of the lattice and decrease of its symmetry to orthorhombic. $Nd_{2-x}Sr_xNiO_{4-\delta}$ ceramics exhibit *p*-type metallic-like electrical conductivity at 500-1000°C under oxidizing conditions, with the highest conductivity (290 S/cm at 900°C in air) observed for x = 1.2. High level of oxygen deficiency in Sr-rich $Nd_{2-x}Sr_xNiO_{4-\delta}$ implies enhanced mixed ionic-electronic transport favorable for electrode applications.

1. Introduction

Layered K_2NiF_4-type $Ln_2NiO_{4+\delta}$ (Ln = La, Pr, Nd) nickelates and their derivatives attract significant attention as a promising alternative to the traditional perovskites for use as electrodes in high-temperature solid electrolyte cells. These oxides belong to Ruddlesden-Popper (RP) series with a general formula $A_{n+1}B_nO_{3n+1}$ and n = 1. The structure of Ln_2NiO_4 can be described as a succession of $LnNiO_3$ perovskite layers alternating with LnO rock-salt layers. The great advantage of this structure is the ability to accommodate hyperstoichiometric oxygen via incorporation of excess oxide ions into interstitial sites within the rock-salt layers. Depending on A- and B-site substitutions, temperature and oxygen partial pressure, the oxygen content in these phases can be either hyper- or hypostoichiometric resulting in the presence of oxygen interstitials or vacancies as point defects responsible for ionic transport.[1] K_2NiF_4-type nickelates were demonstrated to exhibit high oxygen-ion diffusivity,[1-3] acceptable electrical conductivity,[3-5] moderate thermal expansion coefficients [1,3,6-8] and negligible chemical expansion.[8-10] Taking into account the combination of these properties, RP nickelates and in particular $Nd_2NiO_{4\pm\delta}$-based mixed conductors are considered as prospective materials for cathodes of solid oxide fuel cells (SOFCs) [1,5,11,12] and protonic ceramic fuel cells (PCFCs),[13] anodes of solid oxide electrolysis cells (SOECs),[14] and oxygen electrodes of reversible SOFC/SOEC devices.[14,15]

At room temperature, parent $Nd_2NiO_{4+\delta}$ nickelate possesses orthorhombic K_2NiF_4-type structure (space group *Fmmm*) [16,17] with oxygen excess $\delta \sim 0.18$-0.22.[2,7,17,18] On heating in air, orthorhombic $Nd_2NiO_{4+\delta}$ undergoes a phase transition to tetragonal structure (space group *I*4/*mmm*) at 520-610°C [3,7,19] accompanied with semiconductor-to-metal transition at ~450-550°C.[4,3,17] The temperature of structural transition depends on oxygen nonstoichiometry and decreases with reducing $p(O_2)$.[7,8,19]

Single-phase region in $Nd_{2-x}Sr_xNiO_{4\pm\delta}$ system was reported to be limited to $x \leq 1.3$,[20] $x \leq 1.4$,[17] or $x \leq 1.67$.[21] Most likely, this discrepancy is caused by different methods and conditions (temperature, atmosphere) of synthesis. Although the system was studied intensively, most of works were focused on structural, magnetic and electrical properties at low temperatures. Substitution by strontium was reported to shift orthogonal-tetragonal and semiconductor-metal transitions to lower temperatures: all compositions with $x \geq 0.2$ possess tetragonal structure at room temperature,[16-18,22] whereas semiconductor-metal transition in $Nd_{2-x}Sr_xNiO_{4\pm\delta}$ with $x > 0.7$ occurs below room temperature.[17,20,22] Increasing strontium content results in a gradual transition from oxygen hyperstoichiometry (for $x <$ 0.4) to oxygen deficiency (for $x \geq 1.0$) at room temperature [8,16,18,20,22] and has a positive effect on electrical conductivity.[4,16,17] Similar to other RP phases, layered structure results in a strong anisotropy of electronic transport,[23] oxygen-ion diffusion and surface exchange coefficients.[2]

Very limited number of available literature reports on electrochemical properties of $Nd_{2-x}Sr_xNiO_{4+\delta}$-based electrodes focused on Nd-rich side of the series and demonstrated rather mixed results.[6,24,25] Sun et al. [6] found out that

the substitution of neodymium by strontium in $Nd_{2-x}Sr_xNiO_{4\pm\delta}$ (x = 0-0.8) series may improve electrochemical performance in contact with $Ce_{0.9}Gd_{0.1}O_{2-\delta}$ solid electrolyte as compared to the parent material, especially at lower temperatures, with lowest polarization resistance observed for x = 0.4 (0.93 Ω cm^2 at 700°C in air). Khandale et al. [24] reported the area specific resistance of 0.52 Ω cm^2 for $Nd_{1.8}Sr_{0.2}NiO_{4\pm\delta}$ electrodes in contact with $Ce_{0.9}Gd_{0.1}O_{2-\delta}$ electrolyte under the same conditions. On the contrary, Lee et al. demonstrated that the substitution by strontium results in a significant increase of polarization resistance of composite $Nd_{2-x}Sr_xNiO_{4\pm\delta}$- $Ce_{0.9}Gd_{0.1}O_{2-\delta}$ electrodes in contact with 8mol.% yttria-stabilized zirconia solid electrolyte, from 0.55 Ω cm^2 for x = 0 to 23-29 Ω cm^2 for x = 0.4-0.6 at 800°C.[25]

The present work was aimed to explore high-temperature properties of strontium-rich $Nd_{2-x}Sr_xNiO_{4-\delta}$ ($1.0 \leq x \leq 1.6$) series for potential use as oxygen electrodes in solid oxide fuel cells, electrolyzers and reversible SOFC/SOEC systems. Previously, electrochemical activity of RP nickelates was observed to correlate with the concentration of mobile ionic charge carries and bulk ionic conductivity.[12] On the other hand, thermogravimetric and coulometric titration studies evidenced non-negligible oxygen deficiency in $La_{2-x}Sr_xNiO_{4-\delta}$ ($x \geq 1.0$) at elevated temperatures.[26,27] One may expect therefore that oxygen deficiency in Sr-rich $Nd_{2-x}Sr_xNiO_{4-\delta}$ should promote oxygen-ion transport and consequently electrode performance at 600-900°C. In this work, the emphasis was on the properties relevant for oxygen electrode applications, including structural stability, dimensional changes, oxygen nonstoichiometry and electrical conductivity.

2. Experimental

Powders of $Nd_{2-x}Sr_xNiO_{4-\delta}$ (x = 1.0, 1.2, 1.4 and 1.6) were prepared by Pechini method. Appropriate amounts of Nd_2O_3 (Alfa Aesar, 99.9% purity), pre-dried in air at 1000°C to remove adsorbates, $Sr(NO_3)_2$ (Sigma Aldrich, 99% purity) and $Ni(NO_3)_2{\cdot}6H_2O$ (Sigma Aldrich, 98% purity) were dissolved in a minimal volume of 1:1 solution of 6M nitric acid and distilled water. Then, citric acid (CA) and ethylene glycol (EG) were added into the solution in a large excess (4 moles of CA and 10 moles EG per one mole of target oxide). Prepared clear solutions were slowly heated to 120°C to obtain viscous gels which were decomposed by slow further heating up to 350°C and maintaining at this temperature for 10 h. The products were calcined at 600-750°C for 12 h in air to remove carbon-based residues. The precursor powders were subsequently pelletized and annealed at 1000°C (5 h) and 1150-1200°C (15-30 h) under flowing oxygen with frequent regrinding until no further changes could be detected by X-ray diffraction (XRD). Finally, the powders were compacted and sintered at 1250°C for 5 h under oxygen atmosphere.

Sintered ceramic samples were cut into rectangular bars and polished for dilatometric and electrical measurements. The experimental density was calculated from the mass and geometric dimensions of the samples.

Powdered samples for structural studies and thermal analysis were prepared by grinding the sintered ceramics in a mortar.

Room-temperature XRD patterns were collected using Rigaku D/MAX-B (CuKα radiation, 2Θ = 20-85°, step 0.02°, 5 s/step) and PANalytical X'Pert Alpha-1 (CuKα1 radiation, 2Θ = 10-90°, step 0.02°, 5 s/step) diffractometers. Variable-temperature XRD studies were performed employing PANalytical X'Pert PRO MRD instrument (CuKα radiation) equipped with an Anton-Parr XRK900 reaction chamber and PANalytical X'Pert PRO diffractometer (CuKα radiation) with AP HTK-16N high-temperature strip chamber (Pt filament). High-temperature XRD patterns were collected in air on temperature cycling between room temperature and 1000°C with heating/cooling rate of 5°C/min and equilibration for 10 min at each temperature before the actual data acquisition. The structural parameters were refined using FullProf software.

Neutron powder diffraction data were collected at the ISIS pulsed neutron and muon facility of the Rutherford Appleton Laboratory (UK), on the WISH diffractometer located at the second target station. The sample (~0.4 g) was loaded into cylindrical (3 mm diameter) vanadium can and studied at room temperature. Rietveld refinement of the crystal structure was performed using FullProf program against the data measured in detector banks at average 2Θ values of 58^o, 90^o, 122^o, and 154^o, each covering 32^o of the scattering plane.

Dilatometric measurements (vertical Linseis L70/2001 instrument) and thermogravimetric analysis (TGA, Setaram SetSys 16/18 instrument, sensitivity 0.4 μg, initial sample weight ~ 0.5 g) were carried out in flowing oxygen, air or argon at 25-1000°C with constant heating/cooling rate of 1-10°C /min or with isothermal equilibration steps. TGA studies were performed using powdered ceramic samples (unless indicated otherwise). In the course of thermogravimetric studies, each data set included equilibration of the sample with air at 950°C. The absolute oxygen content at this reference state (air, 950°C) was determined thermogravimetrically via *in situ* reduction to metallic Ni, coexisting with SrO and Nd_2O_3, in flowing dry 10%H_2-90%N_2 gas mixture at 950-1100°C. Differential scanning calorimetry (DSC) was performed in air at 5°C/min using Netzsch STA 449 F3 instrument. Electrical conductivity was measured by 4-probe DC method as function of temperature at 500-1000°C in air and as function of oxygen partial pressure at 700-900°C in the p(O_2) range 5×10^{-4}-1.00 atm using O_2-N_2 gas mixtures. Oxygen partial pressure in gas mixtures was monitored by electrochemical yttria-stabilized zirconia oxygen sensor.

3. Results and discussion

3.1. Structural characterization

XRD analysis of as-prepared $Nd_{2-x}Sr_xNiO_{4-\delta}$ ceramic materials confirmed the formation of solid solutions with K_2NiF_4-type structure. The compositions with x = 1.2-1.6 were phase-pure, while trace amounts of NiO phase were

observed in XRD pattern of $NdSrNiO_{4-\delta}$ ceramics (Fig.1) even after additional calcinations of precursor powder for up to 70 h at 1230°C in oxygen flow. The intensity of NiO reflections was however less than 1% of intensity of strongest (*103*) reflection of K_2NiF_4-type phase.

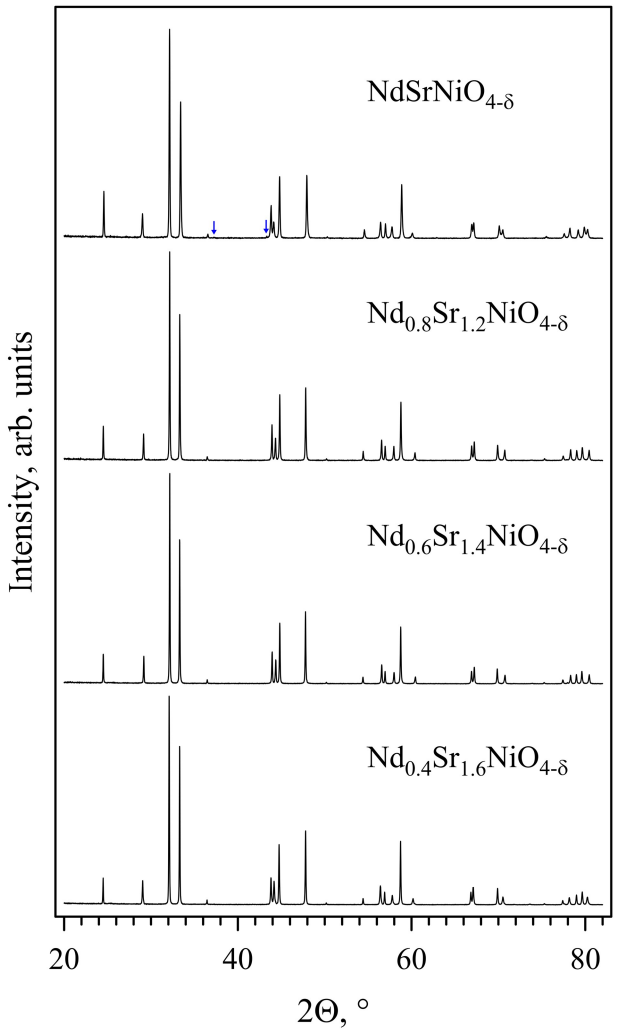

Figure 1. XRD patterns of as-prepared $Nd_{2-x}Sr_xNiO_{4-\delta}$ ceramics. Arrows mark the reflections of NiO impurity.

Table 1

Unit cell parameters and density of as-prepared $Nd_{2-x}Sr_xNiO_{4-\delta}$ ceramics

x	Unit cell parameters				Density, g/cm^3	Relative density, %
	a, Å	c, Å	c/a	V, Å^3		
1.0	3.7951(1)	12.3183(1)	3.246	177.417(2)	6.64	79
1.2	3.8037(1)	12.2587(1)	3.223	177.358(2)	6.43	89
1.4	3.8064(1)	12.2528(1)	3.219	177.527(1)	6.21	83
1.6	3.8038(1)	12.2957(1)	3.232	177.906(2)	5.99	80

XRD patterns of all compositions were successfully indexed using tetragonal *I*4/*mmm* space group, in agreement with the literature data.[16,17,20,21] Refined lattice parameters and unit cell volume (Table 1) showed very minor variations with strontium content and followed the trend reported in literature:[17,21] in the studied compositional range, *a* and *c* parameters show maximum and minimum, respectively, for x = 1.4, with minimum tetragonality ratio *c*/*a* for this composition.

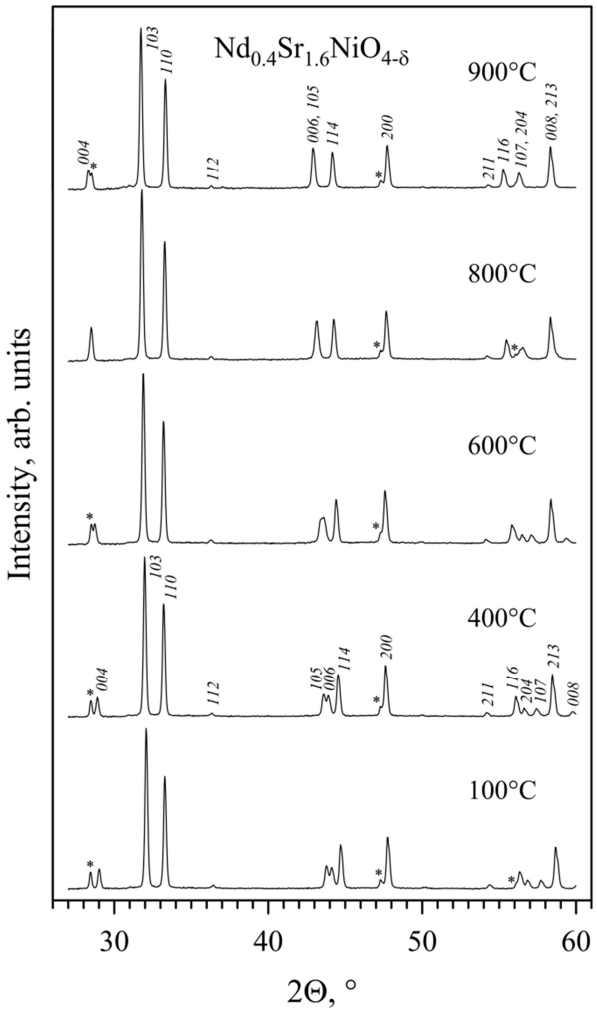

Figure 2. XRD patterns of $Nd_{0.4}Sr_{1.6}NiO_{4-\delta}$ ceramics recorded at different temperatures. Reflections are indexed in *I*4/*mmm* space group. Asterisks mark the peaks of Si standard. Anisotropic lattice expansion results in overlapping of some reflections of K_2NiF_4-type phase at higher temperatures.

Variable-temperature XRD studies at 25-1000°C confirmed that $Nd_{2-x}Sr_xNiO_{4-\delta}$ (x = 1.0-1.6) nickelates preserve tetragonal *I*4/*mmm* structure in this temperature range under oxidizing conditions. As an example, Fig.2 demonstrates XRD patterns for a composition with the highest strontium content. Thermal analysis confirmed the absence of phase transitions under these conditions: no thermal events can be observed in DSC curves on temperature cycling within the

sensitivity of DSC equipment. $Nd_{2-x}Sr_xNiO_{4-\delta}$ exhibit strongly anisotropic lattice expansion on heating: faster elongation along *c* axis as compared to *a-b* plane (Fig.3). Furthermore, increasing strontium content results in progressing deviations of temperature dependencies of the lattice parameters from the linear behavior and eventually even in a lattice contraction in the basal plane at higher temperatures. Such behavior originates from the oxygen nonstoichiometry variations, as discussed below, and has an effect on thermomechanical and electrical properties of these materials.

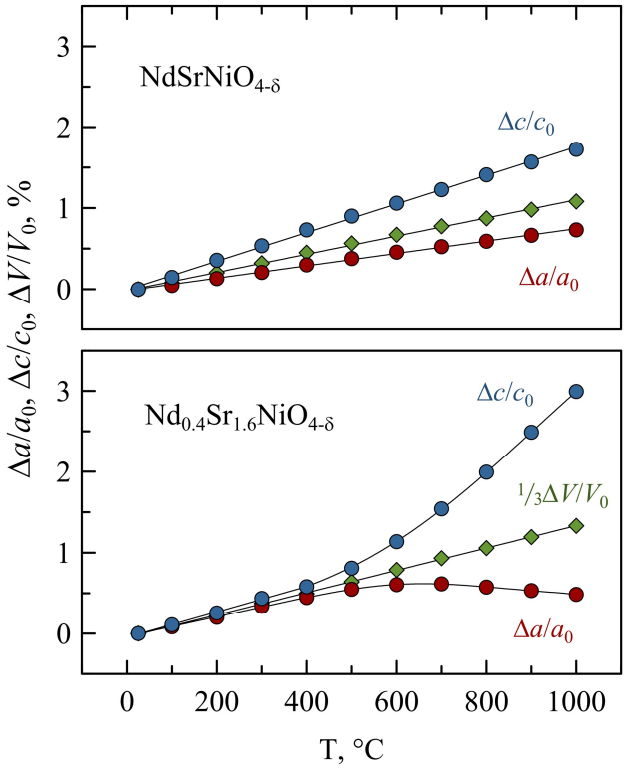

Figure 3. Temperature dependence of unit cell parameters of $NdSrNiO_{4-\delta}$ and $Nd_{0.4}Sr_{1.6}NiO_{4-\delta}$ tetragonal lattice in air.

As-prepared ceramic samples were comparatively porous, with a density of 79-89% of the theoretical (Table 1). Fig.4(A-C) illustrates microstructures of sintered ceramics; the grain sizes were in the range ~1.3-9.0 μm. The difficulties in preparation of dense polycrystalline $Ln_{2-x}Sr_xNiO_{4-\delta}$ samples with $x \geq 1.0$ were noted earlier in literature reports.[28] Attempts to fabricate dense ceramics in this work were not successful as well. Increasing sintering temperature to 1350-1400°C resulted in a rapid grain growth and embrittlement of the samples. Most likely, this is associated with the strongly anisotropic expansion of the grains, especially at higher temperatures, producing significant stresses in polycrystalline samples on cooling and promoting the development of multiple, mostly intergranular, cracks (Fig.4D).

3.2. Oxygen nonstoichiometry under oxidizing conditions

Figure 5 shows variations of oxygen nonstoichiometry in $Nd_{2-x}Sr_xNiO_{4-\delta}$ under oxidizing conditions. The compositions with x = 1.0-1.4 tend to oxygen stoichiometry or even a slight oxygen excess at lower temperatures, < 500-700°C, while $Nd_{0.4}Sr_{1.6}NiO_{4-\delta}$ is oxygen deficient in the entire studied temperature range. On heating, all materials lose oxygen and exhibit oxygen hypostoichiometry; the onset of oxygen losses shifts to lower temperature with increasing strontium content. The range of oxygen nonstoichiometry variations progressively increases with the strontium substitution and with reducing oxygen partial pressure. For x = 1.6, oxygen deficiency δ at 1000°C in air is as high as 0.45 oxygen atoms per formula unit (nearly 1/8 of regular oxygen sites are vacant). Although experimental determination of ionic conductivity was not possible due to porosity of ceramic samples, high concentration of oxygen vacancies implies significant level of oxygen-ionic transport in these materials which should improve with the strontium content.

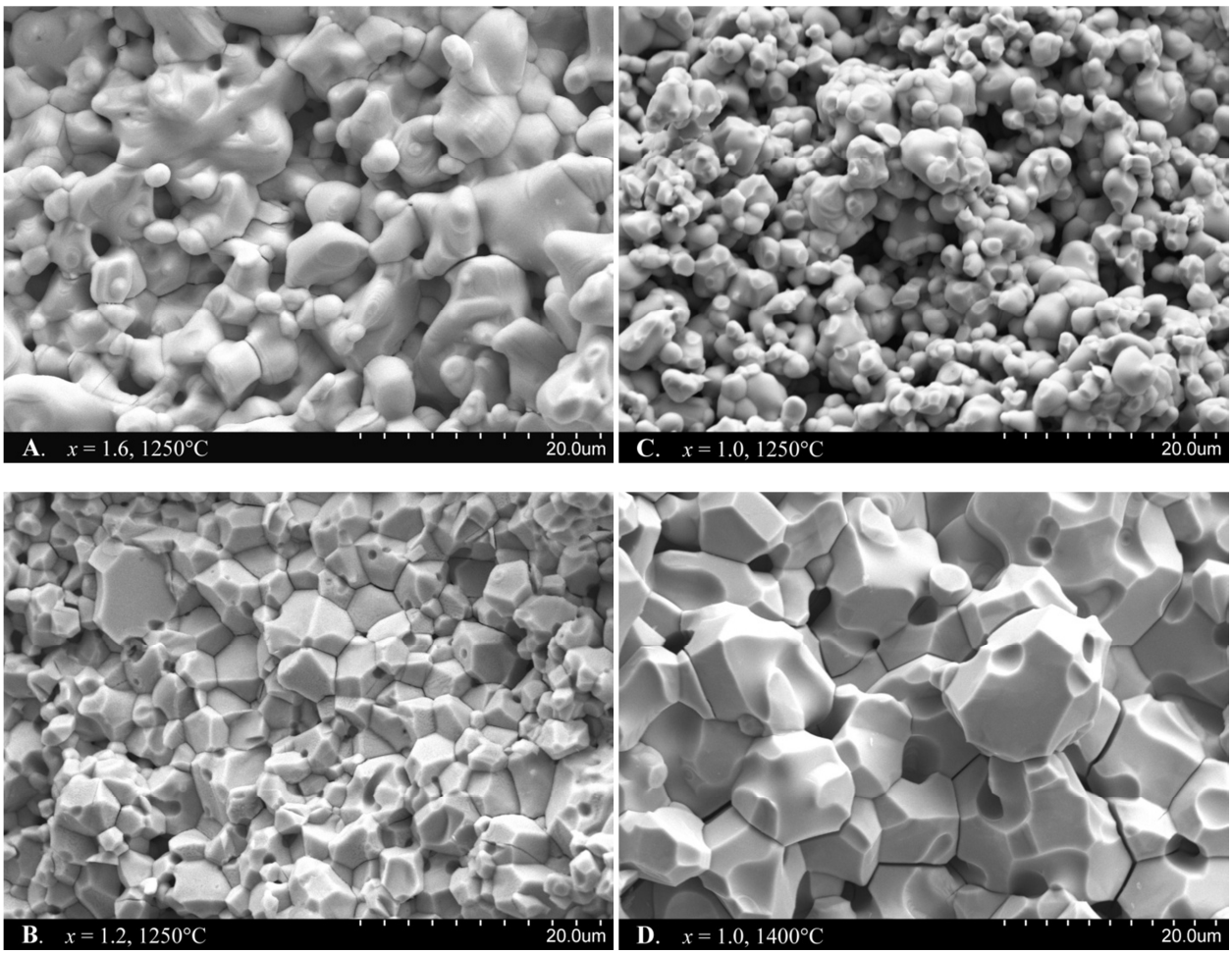

Figure 4. SEM micrographs of fractured $Nd_{2-x}Sr_xNiO_{4-\delta}$ ceramics: (A) x = 1.6, (B) x = 1.2 and (C) x = 1.0 sintered at 1250°C, and (D) x = 1.0 sintered at 1400°C.

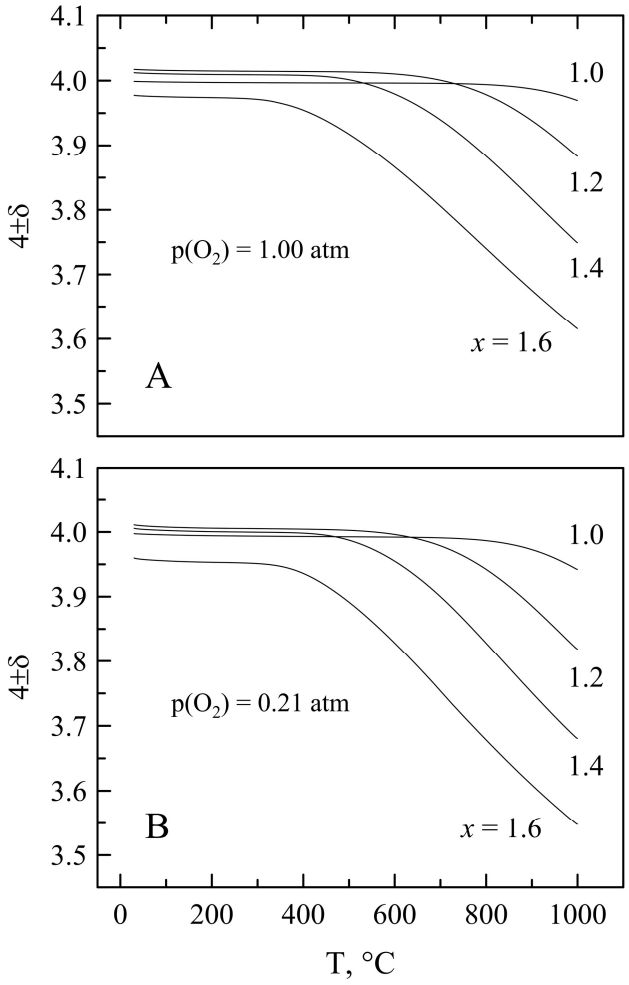

Figure 5. Temperature dependence of oxygen nonstoichiometry of $Nd_{2-x}Sr_xNiO_{4-\delta}$ in oxygen (A) and in air (B).

Acceptor-type substitution by strontium into neodymium sublattice of $Nd_2NiO_{4+\delta}$ can be compensated by changing the concentration of oxygen defects (interstitial oxygen ions or vacancies in oxygen sublattice) and/or by generation of electron-holes. Considering Ni^{3+} and Ni^{4+} equivalent to electron-holes residing on nickel cations and neglecting interstitial oxygen, electroneutrality conditions for strontium-rich $Nd_{2-x}Sr_xNiO_{4-\delta}$ can be expressed as

$$[Sr'_{Nd}] = [Ni^{\bullet}_{Ni}] + 2[Ni^{\bullet\bullet}_{Ni}] + 2[V^{\bullet\bullet}_{O}] = p + 2\delta \quad (1)$$

where p is the concentration of electron-holes per formula unit. Fig.6 shows the average formal valence of nickel cations and electron-hole concentration in $Nd_{2-x}Sr_xNiO_{4-\delta}$ in air calculated from the oxygen nonstoichiometry data assuming that oxygen ions are doubly charged. The results show that mixed Ni^{2+}/Ni^{3+} state is expected only at temperature above ~ 750-800°C. At lower temperature, the average oxidation state of nickel cations tends to 3+ in $NdSrNiO_4$, while for other compositions nickel should be in mixed 3+/4+ oxidation state. One should note that nickel in the 4+ oxidation state is rather unusual for oxide materials. It can be expected, for instance, in perovskite-type $ANiO_3$

(A = Sr, Ba),[29,30] and also was evidenced in $LaGa_{0.65}Mg_{0.15}Ni_{0.20}O_{3-\delta}$ under oxidizing conditions [31] and in $La_{0.9}Sr_{0.1}NiO_{3\pm\delta}$ prepared under elevated oxygen pressure.[32] On the other hand, it is argued that equilibria

$$Ni^{4+} + O^{2-} \leftrightarrow Ni^{3+} + O^{-} \quad (2)$$

$$Ni^{3+} + O^{2-} \leftrightarrow Ni^{2+} + O^{-} \quad (3)$$

are shifted to the right in Ruddlesden-Popper $Ln_{2-x}Sr_xNiO_{4\pm\delta}$ nickelates [28,33] or, in other words, electron-holes may reside in O 2*p* rather than in Ni 3*d* orbitals; this seems to be supported by the X-ray absorption spectroscopy data.[34-36]

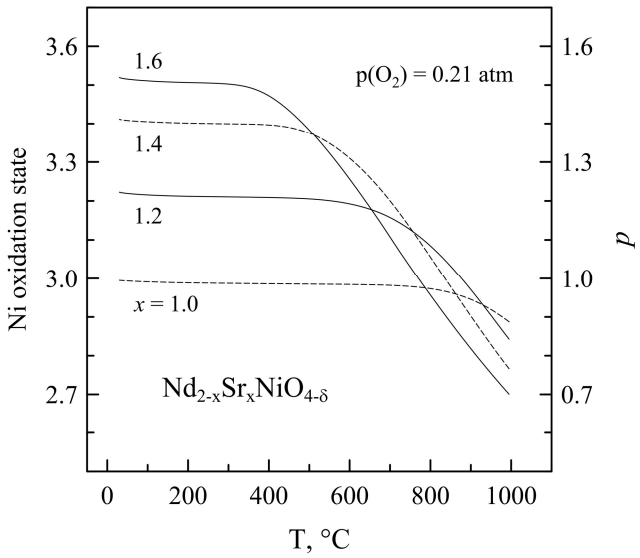

Figure 6. Temperature dependence of formal nickel oxidation state and electron-hole concentration in $Nd_{2-x}Sr_xNiO_{4-\delta}$ in air.

One should emphasize also that all studied $Nd_{2-x}Sr_xNiO_{4-\delta}$ ceramics demonstrated very fast re-equilibration with a gas atmosphere on temperature cycling in the high-temperature range (> 600°C) under oxidizing conditions, as demonstrated by thermogravimetric studies in air and in O_2 (see Electronic supplementary information, Fig.S1). No hysteresis in oxygen nonstoichiometry curves was observed during heating/cooling cycles.

3.3. Structural changes in inert atmosphere

Fig.7 shows variations of oxygen nonstoichiometry in $Nd_{2-x}Sr_xNiO_{4-\delta}$ in one heating/cooling cycle in argon flow at 25-1000°C. As under oxidizing conditions, the oxides lose oxygen from the lattice on heating above ~ 400°C, although the extent of oxygen content variations is higher under reduced $p(O_2)$. Oxygen uptake on cooling was however comparatively small, at least partly due to low oxygen concentration in the gas phase. After cooling, all samples

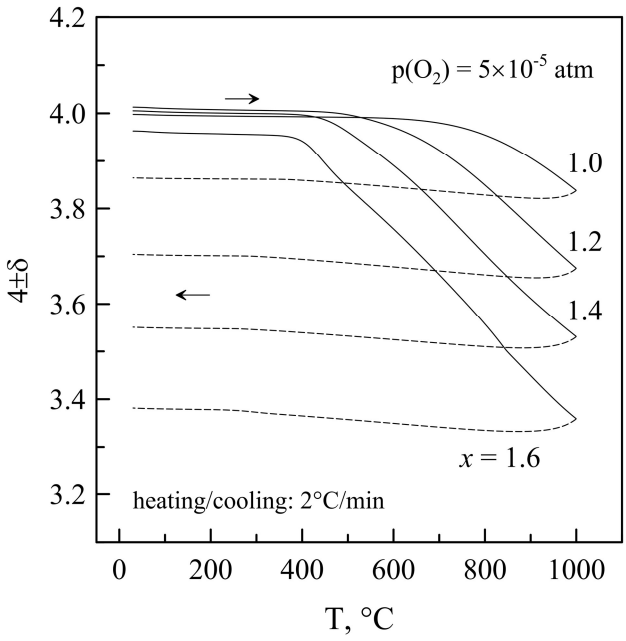

Figure 7. Variations of oxygen nonstoichiometry in air-equilibrated $Nd_{2-x}Sr_xNiO_{4-\delta}$ on heating (solid lines) and subsequent cooling (dashed lines) in argon flow.

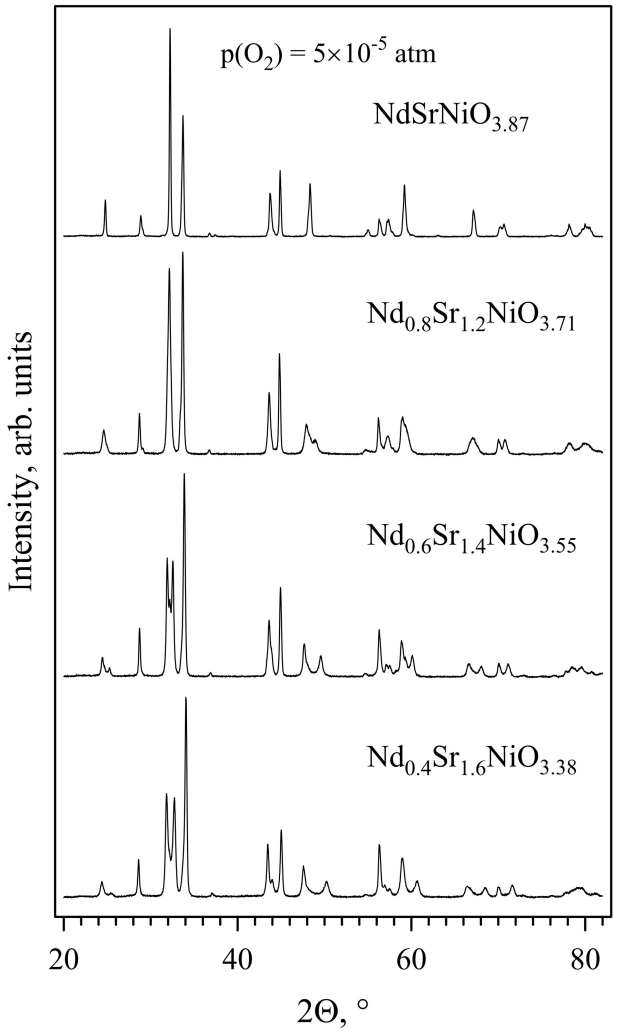

Figure 8. XRD patterns of $Nd_{2-x}Sr_xNiO_{4-\delta}$ ceramic samples after one heating/cooling cycle in argon flow.

exhibited noticeable oxygen deficiency increasing with Sr content. Oxygen losses were accompanied with a decrease of average oxidation state of nickel cations which varied from 2.74+ for x = 1.0 to 2.36+ for x = 1.6 at room temperature.

Results of XRD analysis indicated that $NdSrNiO_{3.87}$ preserves tetragonal *I*4/*mmm* structure after this treatment. The splitting of several reflections in XRD patterns of other compositions suggested however a decrease of the lattice symmetry (Fig.8). This splitting becomes more evident with increasing strontium content (and oxygen deficiency).

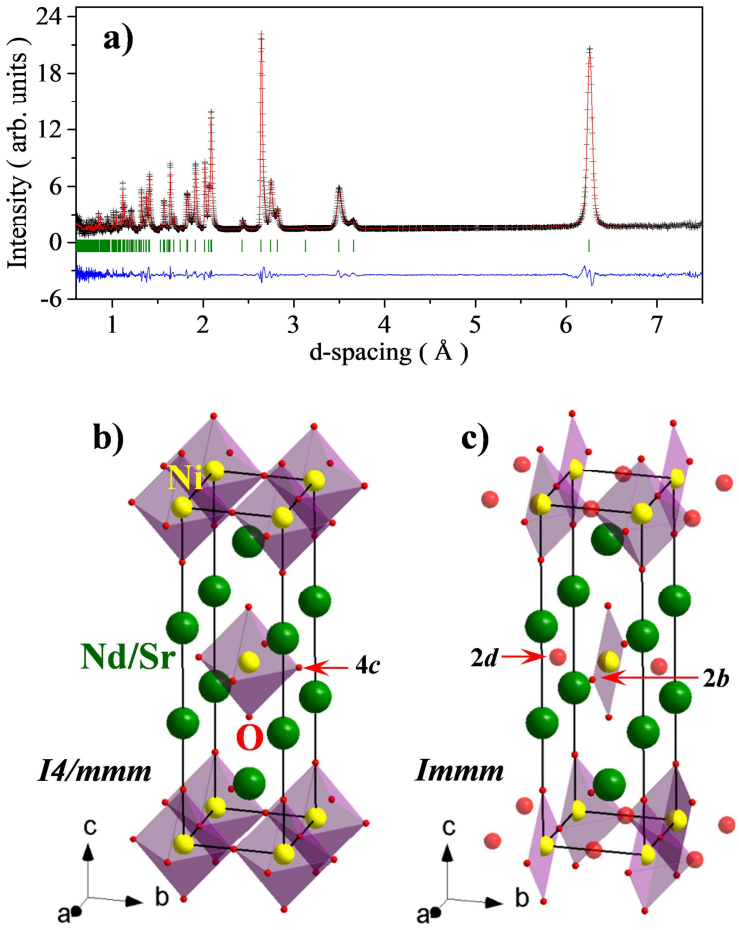

Figure 9. (A) Rietveld refinement of the neutron diffraction data (90-degree WISH detectors bank) collected at 300 K. The cross symbols and the solid line (red) represent the experimental and calculated intensities, respectively, and the line below (blue) is the difference between them. Tick marks (green) indicate the positions of Bragg peaks in the *Immm* space group. Schematic representation of the stoichiometric tetragonal (B) and the oxygen-deficient orthorhombic (C) crystal structures of $Nd_{0.4}Sr_{1.6}NiO_{4-\delta}$ (note that the shown orthorhombic cell is just an illustrative example of the different Ni coordination and does not possess the translational symmetry).

Neutron powder diffraction was employed to determine precisely the crystal structure of reduced $Nd_{0.4}Sr_{1.6}NiO_{4-\delta}$ sample. The room temperature pattern (Fig.9A) revealed a substantial splitting of some of the reflections consistent with

an orthorhombic metric ($a_O > b_O \approx a_T$, $c_O \approx c_T$) of the unit cell. This observation combined with the lack of any superstructure in both X-ray and neutron diffraction data pointed to the *Immm* subgroup as the primary candidate for the crystal structure symmetry of the reduced composition. The *I*4/*mmm*→*Immm* symmetry reduction takes into account the variation of the e_{xx} and e_{yy} macroscopic strains and does not require any changes in the translation symmetry. There are no atomic displacement modes which can drive the symmetry change and the only relevant microscopic order parameter is an order-disorder type. This order parameter is a scalar function localized on the 4*c*(1/2,0,1/2) Wyckoff position of the tetragonal structure (Fig. 9B), which splits it into two sites 2*d*(1/2,0,1/2) and 2*b*(0,1/2,1/2) in the *Immm* subgroup. This scalar order parameter implies a different occupation probability for these positions which in turn means that the reduction procedure creates an oxygen-vacancy ordered structure. Indeed, the quantitative structure refinement confirmed the orthorhombic *Immm* model (Fig.9A) and revealed that the 2*d*(1/2,0,1/2) position is only partially occupied (~27%), whereas the other two oxygen sites do not show any detectable deviations from the stoichiometry. The refined structural parameters are summarized in Table 2, and a schematic illustration of the structure is shown in Figure 9C. The diffraction patterns were considerably affected by microstructural effects resulting in anisotropic peak broadening which has been successfully modelled by a spherical harmonics expansion of the crystallites shape.

Table 2

Atomic coordinates and isotropic thermal parameters for $Nd_{0.4}Sr_{1.6}NiO_{4-\delta}$ at room temperature, refined in the *Immm* space group. Unit cell parameters: a_o = 3.8244(1) Å, b_o = 3.6396(1) Å and c_o = 12.5057(2) Å, R_{Bragg} = 3.03 %.

Atom	Site	*x*	*y*	*z*	Occupancy	*B*
Nd	4*i*	0.5	0.5	0.1452(2)	0.2	1.60(9)
Sr	4*i*	0.5	0.5	0.1452(2)	0.8	1.60(9)
Ni	2*a*	0	0	0	1	1.8(1)
O1	2*d*	0.5	0	0.5	0.27(2)	2.0(1)
O2	2*b*	0	0.5	0.5	1	2.0(1)
O3	4*i*	0	0	0.1571(2)	1	1.19(9)

The structural model implies that Ni cations randomly adopt three different coordinations in the lattice, namely, square planar (coordination number 4), pyramidal (coordination number 5) and octahedral (coordination number 6) with the probabilities 0.53, 0.40 and 0.07, respectively (Fig. 9C). The crystal structure is closely related to the structure of the Ni^{1+}-containing strongly reduced $La_{1.6}Sr_{0.4}(Ni^{1+}_{0.66}Ni^{2+}_{0.34})O_{3.47}$ nickelate [37] as well as to the orthorhombic structure of

Sr_2CuO_3.[38] The latter adopts the same *Immm* space group but the 2*d* Wyckoff position is fully vacant, resulting in a set of isolated chains of Cu ions in the square planar coordination. Other studied compositions of the $Nd_{2-x}Sr_xNiO_{4-\delta}$ series with x = 1.2-1.4 and possibly with x = 1.0 exhibit similar oxygen vacancy ordering after reduction under inert atmosphere. It is remarkable that oxygen-deficient compositions of these series with smaller x, like for instance $Nd_{1.8}Sr_{0.2}NiO_{4-\delta}$, crystalize in a different oxygen vacancy-ordered structure with monoclinic *C2/c* symmetry.[39] Another comment is that, although compositions with $x > 1.0$ show high oxygen deficiency at elevated temperatures in air, they still preserve tetragonal *I4/mmm* structure under oxidizing conditions (Fig.2). This indicates that structural transition is induced not only by the high concentration of oxygen vacancies, but also may be interrelated with the nickel oxidation state.

One should also note that the values of oxygen nonstoichiometry observed during the heating/cooling cycle in inert atmosphere (Fig.7) are not equilibrium. Contrary to oxidizing conditions, $Nd_{2-x}Sr_xNiO_{4-\delta}$ samples demonstrated quite slow kinetics of equilibration in inert gas atmosphere even at 700-950°C (see Electronic supplementary information, Fig.S2). While on cooling this can partly be explained by low concentration of oxygen in the gas flow, slow equilibration on heating implies that in fact this is associated with slow structural changes and that oxygen vacancy ordering is probably accompanied with ordering in cation sublattice as well. The structural changes were found to be reversible: for all compositions, tetragonal structure was restored after annealing in air at 1000°C for 5-10 h.

3.4. Thermochemical expansion

All studied $Nd_{2-x}Sr_xNiO_{4-\delta}$ ceramics exhibit rather unusual dilatometric behavior on thermal cycling under oxidizing conditions (Fig.10). Initially, heating under air or oxygen atmospheres results in a linear elongation of ceramic samples. This is followed however by a noticeable deviation from the linearity above 500-650°C for compositions with $x \geq 1.2$ and even some shrinkage at 750-810°C for ceramics with higher strontium content under air atmosphere. The onset of deviations from a linear expansion shifts to a lower temperature and their extent becomes larger with increasing strontium content. All compositions, including $NdSrNiO_{4-\delta}$, show significant hysteresis in dimensional changes on temperature cycling, although initial dimensions are eventually restored after cooling.

Reversible abrupt dimensional changes in oxide materials on temperature cycling often originate from temperature-induced phase and structural transitions. For nickel-based oxides, relevant examples of such behavior include $Er_{0.3}Sr_{0.7}NiO_{3-\delta}$,[40] $Nd_{1-x}Eu_xNiO_3$ [41] and $BiNiO_3$.[42] However, as mentioned above, thermal analysis did not reveal any thermal events in DSC curves of $Nd_{2-x}Sr_xNiO_{4-\delta}$ ceramic samples. Furthermore, no discontinuity is observed in temperature dependencies of the lattice parameters calculated from the HT-XRD data (Fig.3). All this rules out a phase/structural transition as a cause of specific dilatometric behavior of $Nd_{2-x}Sr_xNiO_{4-\delta}$ ceramics. Other reasons such as

slow lattice relaxation due to sluggish oxygen exchange with a gas phase or excessively fast heating/cooling also can be excluded. As discussed above, $Nd_{2-x}Sr_xNiO_{4-\delta}$ exhibit very fast re-equilibration with a gas phase on temperature cycling. In addition, dilatometric studies with isothermal equilibration steps at 700-950°C demonstrated that, even though ceramic samples show some minor dimensional relaxation during isothermal treatments, these changes are negligible, and the overall shape of dilatometric curves and thermal hysteresis are maintained (see Electronic supplementary information, Fig.S3).

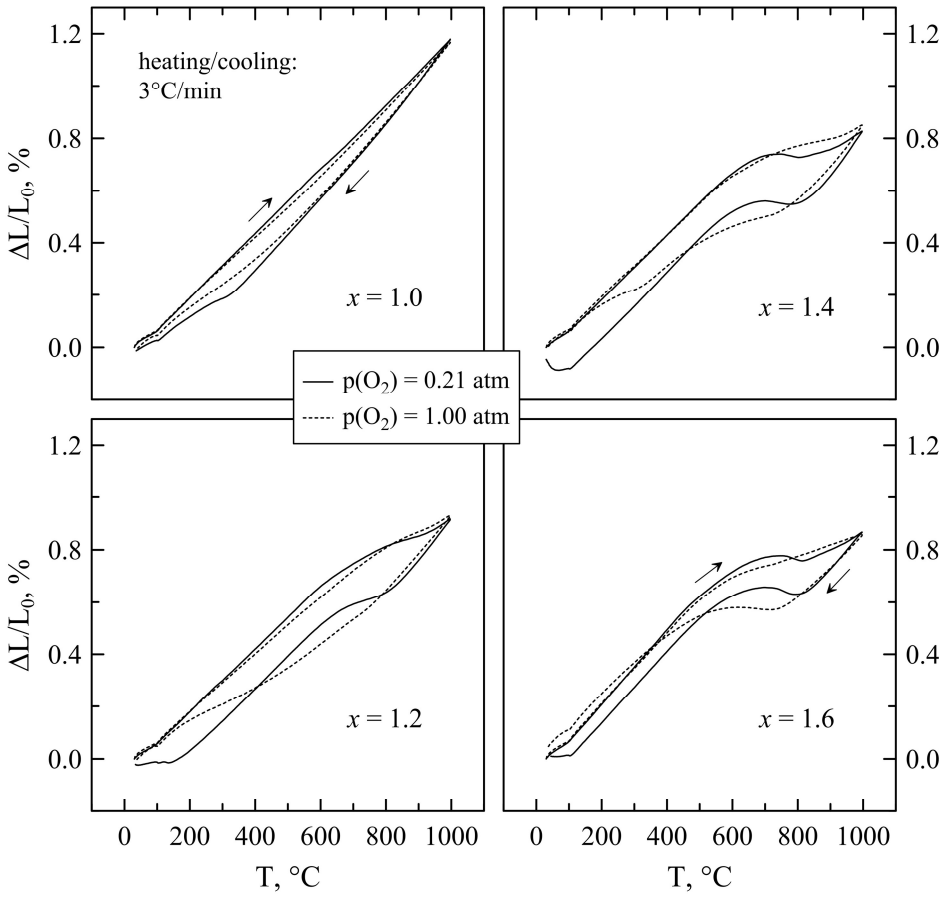

Figure 10. Dilatometric curves of $Nd_{2-x}Sr_xNiO_{4-\delta}$ ceramics on thermal cycling in air (solid lines) and in O_2 (dashed lines).

It turns out, therefore, that the most likely cause of unusual dilatometric behavior of $Nd_{2-x}Sr_xNiO_{4-\delta}$ ceramics is strongly anisotropic behavior of oxygen-deficient K_2NiF_4-type lattice in combination with microcracking. As shown in Fig.3, $Nd_{2-x}Sr_xNiO_{4-\delta}$ demonstrate anisotropic expansion of the lattice on heating with faster elongation along *c* axis as compared to the basal plane dimensions. Although the unit cell volume increases linearly with temperature, anisotropic expansion of differently oriented individual grains in polycrystalline samples induces internal strains which cannot be accommodated by pores and promote the development of microcracks on cooling from strain-free state at sintering

temperature. Microcracking is known to be a cause of a large hysteresis in thermal expansion curves of ceramic materials with a crystallographic anisotropy;[43,44] one typical example is aluminum titanate Al_2TiO_5.[45] Heating above a certain temperature results in "healing" of microcracks and deviation from the linear behavior and even some contraction. On cooling, anisotropic strain mismatch is compensated by re-opening of microcracks which has an opposite effect on dilatometric curves. As microcracks healing and re-opening initiates at different temperatures on heating and cooling, this results in a hysteresis in dilatometric curves. Dilatometric data (Fig.10) suggest the microcracking-related processes in the studied nickelates occur mostly at ~600-800°C, although initial dimensions of the samples are restored only after cooling down to room temperature due to slow microstructural relaxation. This phenomenon reasonably explains unusual dilatometric behavior of $Nd_{2-x}Sr_xNiO_{4-\delta}$ samples as well as embrittlement of the ceramics sintered at higher temperatures (due to grain growth followed by a stronger microcracking on cooling).

Dimensional changes are closely interrelated with the oxygen nonstoichiometry variations. Increasing strontium content gives rise to larger oxygen nonstoichiometry changes (Fig.5) and consequently higher anisotropicity of the lattice expansion on heating (Fig.3). For Sr-rich compositions, temperature dependencies of the lattice constants deviate from a linear behavior, and these deviations have opposite trends for *a* and *c* parameters; eventually, a contraction in *a*-*b* plane is observed at higher temperatures. As a result, increasing *x* results in larger dimensional changes in $Nd_{2-x}Sr_xNiO_{4-\delta}$ ceramics at 700-900°C. On the contrary, increasing $p(O_2)$ reduces variations of δ with temperature and has a reverse effect on dimensional changes.

Note that, although lattice anisotropy and accompanying microcracking phenomenon hinder the fabrication of dense ceramic samples, these factors can be expected to have a rather minor effect on thermomechanical stability of electrode layers due to smaller grain size and significant fraction of pores (≥ 40 vol.%) which can accommodate the strains. Besides, studied $Nd_{2-x}Sr_xNiO_{4-\delta}$ ceramics seem to possess moderate thermal expansion coefficients (TECs). Table 3 lists average TEC values calculated from the dilatometric data (straight segments on heating) and from the high-temperature XRD data. These values are in good agreement with the data reported for other $Nd_{2-x}Sr_xNiO_{4-\delta}$ ceramics (x = 0-0.8, $\bar{\alpha}$ = (11.6-14.4)×10^6 K^{-1})[3,6,8] and also are comparable with TECs of common solid electrolytes (such as stabilized zirconia, doped ceria or substituted lanthanum gallate) thus ensuring their thermomechanical compatibility.

Fig.11 compares dimensional changes of $NdSrNiO_{4-\delta}$ and $Nd_{0.4}Sr_{1.6}NiO_{4-\delta}$ ceramics in one heating/cooling cycle in air and in inert atmosphere. Oxygen losses on thermal cycling at reduced $p(O_2)$ lead to a contraction of ceramic samples; the magnitude of these dimensional changes is strongly correlated the range of oxygen nonstoichiometry variations increasing with *x* (Fig.7).

Chemical-induced dimensional changes on reduction of oxide materials with variable-valence cations originate from two simultaneous competing processes: (i) formation of oxygen vacancy leading to lattice contraction due to electrostatic interactions, and (ii) simultaneous increase of cation radius causing lattice expansion due to steric effects.[46] As the second process has a stronger impact, oxygen losses on temperature and $p(O_2)$ changes result in overall dilation of crystal lattice in the case of perovskite and fluorite structures.[47,48]

Table 3

Average thermal expansion coefficients of $Nd_{2-x}Sr_xNiO_{4-\delta}$ ceramics

x	Method	T range, °C	$\bar{\alpha} \times 10^6$, K^{-1}	
			$p(O_2)$ = 0.21 atm	$p(O_2)$ = 1.00 atm
1.0	dilatometry	100-1000	12.3	12.2
	HT-XRD	25-1000	11.1	
1.2	dilatometry	100-600	12.1	11.8
1.4	dilatometry	100-600	12.3	11.9
1.6	dilatometry	100-470	14.3	13.6
	HT-XRD	25-1000	13.6	

Note: TEC values caluclated from the dilatometric data correspond to straight segments on heating.

The situation is different for anisotropic K_2NiF_4-type nickelates. Previous studies of oxygen-overstoichiometric $Ln_2NiO_{4+\delta}$ -based ceramic materials demonstrated that decreasing oxygen excess in these materials under isothermal conditions results in increasing *a* and decreasing *c* parameters; these changes compensate each other resulting in nearly constant unit cell volume and negligible chemical expansion/contraction on redox cycling.[8-10] It turns out that in oxygen-deficient $Nd_{2-x}Sr_xNiO_{4-\delta}$ nickelates, within tetragonal phase domain, lattice parameters vary in a different way: *a* decreases and *c* increases with increasing δ, though these changes still compensate each other as follows from a linear behavior of unit cell volume (Fig.3). This is in agreement with available literature data on $LaSrNiO_{4-\delta}$.[27]

High oxygen losses under inert gas atmosphere result, as expected, in dilation of $Nd_{0.4}Sr_{1.6}NiO_{4-\delta}$ lattice along *c* axis (see Tables 1 and 2). At the same time, ordering in oxygen sublattice causes distortion of the structure and significant contraction along b_O axis. Although the size of nickel cation should increase on reduction, it simultaneously decreases with decreasing coordination number,[48] resulting in a net contraction in basal plane and shrinkage of unit cell volume. Similar behavior is characteristic for other $Nd_{2-x}Sr_xNiO_{4-\delta}$ ceramics diminishing when strontium content decreases. Interestingly, dilatometric curve of $Nd_{0.4}Sr_{1.6}NiO_{4-\delta}$ on cooling in argon, when oxygen nonstoichiometry is

almost constant (Fig.7), did not show any anomalous behavior (Fig.11) once again confirming that the unusual behavior of dilatometric curves under oxidizing conditions is correlated with significant oxygen losses.

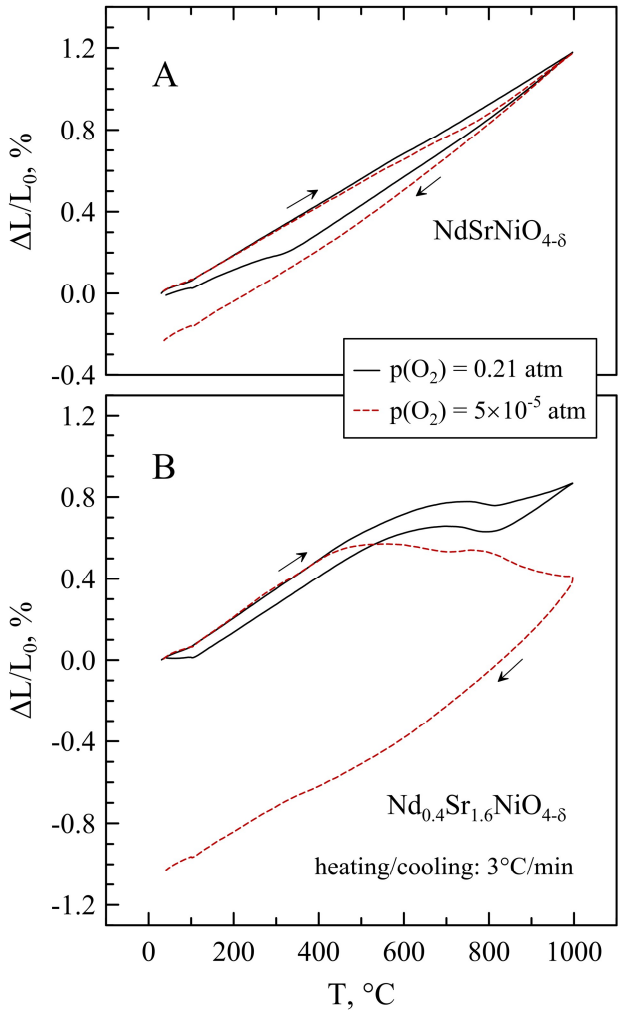

Figure 11. Dilatometric curves of $NdSrNiO_{4-\delta}$ (A) and $Nd_{0.4}Sr_{1.6}NiO_{4-\delta}$ (B) ceramics in one heating/cooling cycle in air (solid lines) and in argon flow (dashed lines). Before the experiments, the samples were slowly cooled down in air.

3.4. Electrical conductivity

All $Nd_{2-x}Sr_xNiO_{4-\delta}$ (x = 1.0-1.6) ceramics exhibit metallic-like electrical conductivity in the studied temperature range under oxidizing conditions (Fig.12). Conductivity initially increases with strontium content reaching the maximum for x = 1.2 and then decreases on further substitution. For $Nd_{0.8}Sr_{1.2}NiO_{4-\delta}$, the values of conductivity in air are as high as 286 and 510 S/cm at 900°C and 600°C, respectively. All studied materials show higher electrical conductivity if compared to parent $Nd_2NiO_{4+\delta}$.

It is considered that metallic-like conduction in $Ln_{2-x}Sr_xNiO_{4\pm\delta}$ occurs via free electron-holes in the $\sigma_{x^2-y^2}$ band formed by delocalized $d_{x^2-y^2}$ Ni orbitals, while d_{z^2} electrons are localized.[4,17,20,22,28] Increasing temperature decreases

electronic transport in $Nd_{2-x}Sr_xNiO_{4-\delta}$ due to decline of both electron-holes concentration (Fig.6) and their mobility.[4] Variations of electrical conductivity in $Nd_{2-x}Sr_xNiO_{4-\delta}$ (x = 1.0-1.6) series correlates to some extent with calculated electron-hole concentration (Fig.6) but only at higher temperatures, above 800°C, when the formal oxidation state on Ni is close to 3+ or less. It seems therefore that the compositional dependence of electrical conductivity in these series is an interplay between structural parameters, concentration of electron-holes, distribution of electrons between $d_{x^2-y^2}$ and d_{z^2} orbitals, and electron-hole mobility which also may be affected by oxygen nonstoichiometry due to scattering on oxygen vacancies. An additional factor is microstructural effects (porosity, microcracking).

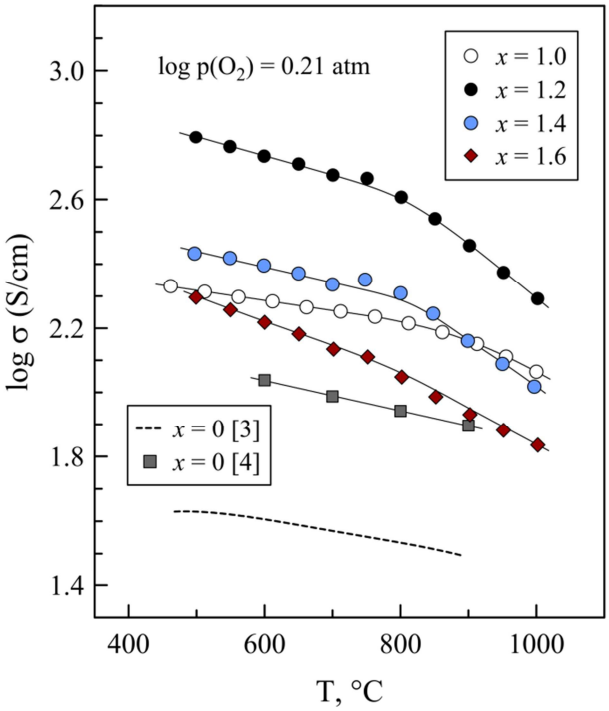

Figure 12. Temperature dependence of electrical conductivity of $Nd_{2-x}Sr_xNiO_{4-\delta}$ ceramics in air. Each data point was obtained after equilibration at given temperature for 4-20 h. Literature data [3,4] on $Nd_2NiO_{4+\delta}$ are shown for comparison; the data points in air [4] were extrapolated from the σ - *log p(O₂)* dependences.

Note that the data shown in Fig.12 are "equilibrium" values, i.e. values obtained in cooling regime after equilibration at each temperature for 4-20 h until the drift of conductivity with time became negligible. On temperature cycling, however, the conductivity curves demonstrate significant hysteresis at 600-1000°C (Fig.13). This apparent hysteresis originates from the dimensional changes accompanied with microcracking, as discussed above; both these factors have an effect on measured conductivity values. As for dilatometric curves (see Electronic supplementary information, Fig.S3B), this quasi-hysteresis cannot be eliminated by isothermal equilibration.

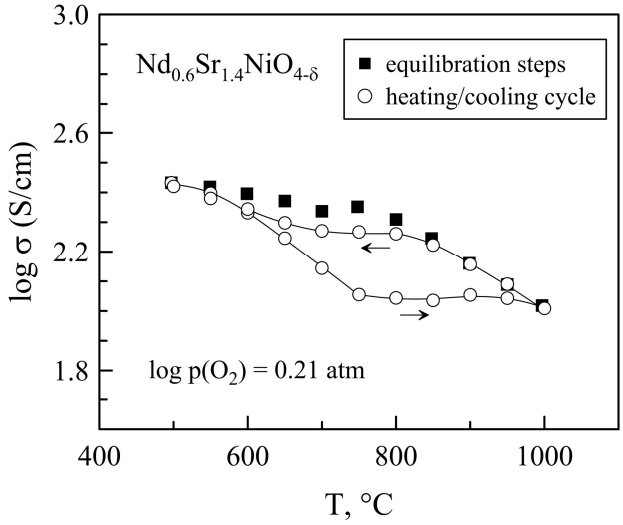

Figure 13. Electrical conductivity of $Nd_{0.6}Sr_{1.4}NiO_{4-\delta}$ ceramics in air: (squares) values obtained in cooling regime with equilibration at each temperature for 4-20 h, and (circles) values measured in a heating/cooling cycle between 500 and 1000°C at 5°C/min.

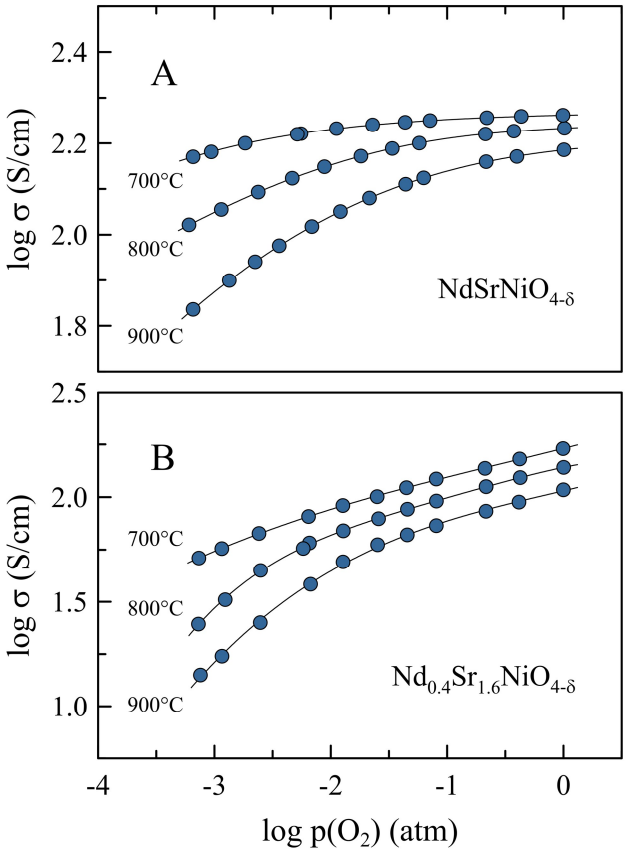

Figure 14. Oxygen partial pressure dependence of electrical conductivity of $Nd_{2-x}Sr_xNiO_{4-\delta}$ ceramics at 700-900°C.

Oxygen partial pressure dependence of electrical conductivity of $Nd_{2-x}Sr_xNiO_{4-\delta}$ ceramics confirms that electronic transport is *p*-type and decreases on reducing $p(O_2)$ (Fig.14) due to oxygen release from the lattice accompanied with elimination of electron-holes:

$$O_O^{\times} + 2h^{\bullet} \leftrightarrow V_O^{\bullet\bullet} + 0.5O_2; \qquad K = \frac{\delta}{4-\delta}\frac{p(O_2)^{1/2}}{p^2} \qquad (4)$$

where *K* is temperature-dependent equilibrium constant. In the studied $p(O_2)$ range, all compositions preserve metallic-like behavior with conductivity decreasing on heating (Fig.14). Electron-hole conductivity is a function of both oxygen partial pressure and oxygen nonstoichiometry (which in turn also depends on $p(O_2)$):

$$\sigma_p = e\mu_p p = e\mu_p \left(\frac{\delta}{4-\delta}\right)^{0.5} K^{-0.5} p(O_2)^{1/4} \qquad (5)$$

and therefore demonstrate strongly non-linear behavior in *log* σ - *log p(O$_2$)* coordinates. Still, all composition exhibit comparatively high level of electronic transport under oxidizing conditions (> 10 S/cm at $p(O_2) > 5\times10^{-4}$ and $T \le 900$°C even for $x = 1.6$) acceptable for oxygen electrode applications. Taking into account the data on oxygen nonstoichiometry (Fig.5), one may expect that Sr-rich $Nd_{2-x}Sr_xNiO_{4-\delta}$ are mixed conductors with non-negligible contribution of oxygen-ion transport to the total electrical conductivity, which is favorable for electrochemical activity.

4. Conclusions

(i) $Nd_{2-x}Sr_xNiO_{4-\delta}$ (x = 1.0-1.6) ceramics with K_2NiF_4-type tetragonal structure were prepared by Pechini method and sintered at 1250°C in oxygen atmosphere. Tetragonal structure is preserved under oxidizing conditions on heating up to 1000°C;

(ii) Acceptor-type substitution by strontium is compensated by electron-holes and oxygen vacancies; the role of the latter increases on heating. Oxygen deficiency at elevated temperature increases with strontium doping reaching ~ 1/8 of oxygen sublattice for $x = 1.6$ at 1000°C in air;

(iii) Strong anisotropy of tetragonal lattice expansion on heating correlated with the oxygen nonstoichiometry variations results in an anomalous dilatometric behavior of $Nd_{2-x}Sr_xNiO_{4-\delta}$ ceramics. The results of dilatometric and high-temperature XRD studies show however moderate average thermal expansion coefficients comparable with that of common solid electrolytes;

(iv) Reduction of $Nd_{2-x}Sr_xNiO_{4-\delta}$ in inert gas atmosphere induces oxygen vacancy ordering accompanied with a decrease of the lattice symmetry down to orthorhombic and contraction of ceramics;

(v) $Nd_{2-x}Sr_xNiO_{4-\delta}$ ceramics possess *p*-type metallic-like electrical conductivity under oxidizing conditions decreasing on reducing oxygen partial pressure. Highest conductivity is observed for $x = 1.2$ reaching 290-510 S/cm at 600-900°C. The level of oxygen deficiency in Sr-rich $Nd_{2-x}Sr_xNiO_{4-\delta}$ implies that these materials are mixed conductors with non-negligible contribution of ionic transport to the total conductivity.

Acknowledgements

This work was developed within the project IF/01072/2013/CP1162/CT0001 and project CICECO-Aveiro Institute of Materials (ref. UID/CTM/50011/2013) financed by national funds through the FCT/MEC and when applicable co-financed by FEDER under the PT2020 Partnership Agreement. Ekaterina Kravchenko gratefully acknowledges the doctoral grant (Belarusian State University) and Visby Programme scholarship (Swedish Institute). Authors are thankful to Alexandre Viskup (RI PCP BSU) and Dr. Aliaksandr Shaula (TEMA/UA) for experimental assistance.

References

1. A. Tarancón, M. Burriel, J. Santiso, S.J. Skinner and J.A. Kilner, *J. Mater. Chem.*, 2010, **20**, 3799-3813.
2. J.-M. Bassat, M. Burriel, O. Wahyudi, R. Castaing, M. Ceretti, P. Veber, I. Weill, A. Villesuzanne, J.-C. Grenier, W. Paulus and J.A. Kilner, *J. Phys. Chem.C*, 2013, **117**, 26466-26472.
3. E. Boehm, J.-M. Bassat, P. Dordor, F. Mauvy, J.-C. Grenier and Ph. Stevens, *Solid State Ionics*, 2005, **176**, 2717-2725.
4. T. Nakamura, K. Yashiro, K. Sato and J. Mizusaki, *Mater. Chem. Phys.*, 2010, **122**, 250-258.
5. G. Amow and S.J. Skinner, *J Solid State Electrochem.*, 2006, **10**, 538-546.
6. L.-P. Sun, Q. Li, H. Zhao, L.-H. Huo and J.-C. Grenier, *J. Power Sources*, 2008, **183**, 43-48.
7. A. Flura, S. Dru, C. Nicollet, V. Vibhu, S. Fourcade, E. Lebraud, A. Rougier, J-M. Bassat and J.-C. Grenier, *J. Solid State Chem*., 2015, **228**, 189-198.
8. T. Nakamura, K. Yashiro, K. Sato and J. Mizusaki, *Solid State Ionics*, 2010, **181**, 402-411.
9. V.V. Kharton, A.V. Kovalevsky, M. Avdeev, E.V. Tsipis, M.V. Patrakeev, A.A. Yaremchenko, E.N. Naumovich and J.R. Frade, *Chem. Mater*., 2007, **19**, 2027-2033.
10. T. Nakamura, Y. Ling and K. Amezawa, *J. Mater. Chem. A*, 2015, **3**, 10471-10479.
11. M.A. Laguna-Bercero, A.R. Hanifi, H. Monzón, J. Cunningham, T.H. Etsell and P. Sarkar, *J. Mater. Chem. A*, 2014, **2**, 9764-9770.
12. A.A. Yaremchenko, V.V. Kharton, D.O. Bannikov, D.V. Znosak, J.R. Frade and V.A. Cherepanov, *Solid State Ionics*, 2009, **180**, 878-885.
13. C. Yang, X. Zhang, H. Zhao, Y. Shen, Z. Du, and C. Zhang, *Int. J. Hydrogen Energy*, 2015, **40**, 2800-2807.
14. F. Chauveau, J. Mougin, J.M. Bassat, F. Mauvy, and J.C. Grenier, *J. Power Sources*, 2010, **195**, 744-749.
15. M.A. Laguna-Bercero, N. Kinadjan, R. Sayers, H. El Shinawi, C. Greaves, S.J. Skinner, *Fuel Cells*, 2011, **11**, 102-107.
16. M.P. Sridhar Kumar, S.M. Doyle and D.M^{c}K Paul, *J. Less-Common Met*., 1990, **164-165**, 920-925.
17. Y. Takeda, M. Nishijima, N. Imanishi, R. Kanno, O. Yamamoto and M. Takano, *J. Solid State Chem*., 1992, **96**, 72-83.
18. J. Alonso, M. Vallet-Regí and J.M. González-Calbet, *Solid State Ionics*, 1993, **66**, 219-223.
19. E. Niwa, T. Nakamura, J. Mizusaki and T. Hashimoto, *Thermochim. Acta*, 2011, **523**, 46-50.
20. S.M. Doyle, M.P. Sridhar Kumar and D.M^{c}K Paul, *J. Phys. Condens. Matter.*, 1992, **4**, 3559-3568.
21. M. James and J.P. Attfield, *J. Mater. Chem*., 1996, **6**, 57-62.
22. B.W. Arbuckle, K.V. Ramanujachary, Z. Zhang and M. Greenblatt, *J. Solid State Chem*., 1990, **88**, 278-290.

23. K. Sugiyama, H. Nozaki, T. Takeuchi and H. Ikuta, *J. Phys. Chem. Solids*, 2002, **63**, 979-982.

24. A.P. Khandale, J.D. Punde and S.S. Bhoga, *J. Solid State Electrochem*., 2013, **17**, 617-626.

25. K.-J. Lee, J.-U. Seo, Y.-S. Lim, H.-J. Hwang, *J. Kor. Ceram. Soc*., 2014, **51**, 51-56.

26. L.V. Makhnach, V.V. Pankov and P. Strobel, *Mater. Chem. Phys* , 2008, **111**, 125-130.

27. V.V. Vashook, N.E. Trofimenko, H. Ullmann and L.V. Makhnach, *Solid State Ionics*, 2000, **131**, 329-336.

28. Y. Takeda, R. Kanno, M. Sakano, O. Yamamoto, M. Takano, Y. Bando, H. Akinaga, K. Takita and J.B. Goodenough, *Mater. Res. Bull*., 1990, **25**, 293-306.

29. Y. Takeda, T. Hashino, H. Miyamoto, F. Kanamaru, S. Kume and M. Koizumi, *J. Inorg. Nucl. Chem*., 1972, **34**, 1599-1601.

30. Y. Takeda, F. Kanamaru, M. Shimada and M. Koizumi, *Acta Crystallogr. B*, 1976, **32**, 2464-2466.

31. E.N. Naumovich, V.V. Kharton, A.A. Yaremchenko, M.V. Patrakeev, D.G. Kellerman, D.I. Logvinovich and V.L. Kozhevnikov, *Phys. Rev. B*, 2006, **74**, 064105.

32. J.A. Alonso, M.J. Martínez-Lope and M.A. Hidalgo, *J. Solid State Chem*., 1995, **116**, 146-156.

33. D. Reinen, U. Kesper and D. Belder, *J. Solid State Chem*., 1995, **116**, 355-363.

34. Z. Hu, M.S. Golden, J. Fink, G. Kaindl, S.A. Warda, D. Reinen, P. Mahadevan and D.D. Sarma, *Phys. Rev. B*, 2000, **61**, 3739-3744.

35. P. Kuiper, J. van Elp, G.A. Sawatzky, A. Fujimori, S. Hosoya and D.M. de Leeuw, *Phys. Rev. B*, 1991, **44**, 4570-4575.

36. A.K. Ganguli, R. Nagarajan, G. Ranga Rao, N.Y. Vasanthacharya and C.N.R. Raot, *Solid State Comm*., 1989, **72**, 195-197.

37. M. Crespin, J.M. Bassat, P. Odier, P. Mouron and J. Choisnet, *J. Solid State Chem.*, 1990, **84**, 165-170.

38. M.T. Weller and D.R. Lines, *J. Solid State Chem*., 1989, **82**, 21-29.

39. M. Medarde, J. Rodríguez-Carvajal, M.; Vallet-Regí, J.M. González-Calbet and J. Alonso, *Phys. Rev. B*, 1994, **49**, 8591-8599.

40. L. Fu, M. Chao, H. Chen, X. Liu, Y. Liu, J. Yu, E. Liang, Y. Li and X. Xiao, *Phys. Lett. A*, 2014, **378**, 1909-1912.

41. M.T. Escote, V.B. Barbeta, R.F. Jardim and J. Campo, *J. Phys. Condens. Matter*, 2006, **18**, 6117-6132.

42. M. Azuma, W. Chen, H. Seki, M. Czapski, O. Smirnova, K. Oka, M. Mizumaki, T. Watanuki, N. Ishimatsu, N. Kawamura, S. Ishiwata, M.G. Tucker, Y. Shimakawa, J.P. Attfield, *Nature Comm*., 2011, **2**, 347.

43. R. Morrell, in *Concise Encyclopedia of Advanced Ceramic Materials*, ed. R.J. Brook, Pergamon Press, New York, 1991, 475-478.

44. W. Höland, G.H. Beall, *Glass-Ceramic Technology, Second Edition*, Wiley, Hoboken, NJ, 2012; pp 304-307.

45. H.A.J. Thomas and R. Stevens, *Br. Ceram. Trans. J.*, 1989, **88**, 144-151.

46. D. Marrocchelli, S.R. Bishop, H.L. Tuller and B. Yildiz, *Adv. Funct. Mater*., 2012, **22**, 1958-1965.

47. A.A. Yaremchenko, S.M. Mikhalev, E.S. Kravchenko and J.R. Frade, *J. Eur. Ceram. Soc.*, 2014, **34**, 703-715.

48. R.D. Shannon, *Acta Cryst. A*, 1976, **32**, 751-767.